e 1

EXPERIMENTAL PRESSURE DROP INVESTIGATION OF WETTING AND NONWETTING MERCURY CONDENSING IN UNIFORMLY TAPERED TUBES

by James A. Albers and Henry B. Block

Lewis Research Center

Cleveland, Ohio

EXPERIMENTAL PRESSURE DROP INVESTIGATION

OF WETTING AND NONWETTING MERCURY CONDENSING

IN UNIFORMLY TAPERED TUBES

By James A. Albers and Henry B. Block

Lewis Research Center
Cleveland, Ohio

NATIONAL AERONAUTICS AND SPACE ADMINISTRATION

EXPERIMENTAL PRESSURE DROP INVESTIGATION OF WETTING AND NONWETTING

MERCURY CONDENSING IN UNIFORMLY TAPERED TUBES

by James A. Albers and Henry B. Block

Lewis Research Center

SUMMARY

An experimental investigation was conducted to compare the pressure drop of wetting and nonwetting mercury condensing in horizontal convectively cooled tubes. The test sections consisted of 4-foot-long tubes uniformly tapered from 0.50- to 0.20-inch nominal inside diameters. Local static pressure data were obtained for condensing lengths from 18 to 45 inches and vapor mass flow rates ranging from 0.025 to 0.052 pounds per second corresponding to inlet velocities of 90 to 190 feet per second.

In general, an overall static pressure rise was obtained for both wetting and nonwetting conditions at the weight flows and condensing lengths considered. At a mass flow rate of 0.028 pound per second, the overall static pressure difference $(P_1 - P_{liq})_S$ was approximately equal for the wetted and nonwetted condensers. At mass flow rates of 0.038 and 0.049 pound per second, $(P_1 - P_{liq})_S$ for nonwetted flow exceeded that for wetted flow by a pressure rise of 0.3 and 0.6 pound per square inch, respectively. This pressure difference between nonwetted and wetted flows was significant compared with the overall pressure recovery.

The Lockhart-Martinelli correlation agreed with the data for qualities greater than 0.4 (i.e., corresponding to low values of the parameter X). For qualities less than 0.4 (i.e., corresponding to high values of the parameter X), the frictional pressure gradient was greater than that predicted by Lockhart-Martinelli, and the deviation increased with an increase in the parameter X. The fog-flow correlation of Koestel agreed with the nonwetted and wetted data for qualities greater than 0.4 (i.e., corresponding to Weber numbers greater than 10). The fog-flow theory roughly predicted the trend of the nonwetting data for qualities less than 0.4 (i.e., corresponding to Weber numbers less than 10) although the frictional pressure gradients were slightly higher than those predicted by theory. The frictional pressure gradients for wetted flow were slightly higher than those for the nonwetted condition in the low-quality region of the condensing tube (last half of the condensing length). This may be due to the fact that the buildup of liquid on the bottom of the tube in wetting condensing (which reduced the effective vapor flow area) was greater than the buildup of drops on the tube wall in nonwetting condensing.

INTRODUCTION

Liquid-metal Rankine-cycle turbogenerator systems are currently being considered for the generation of electric power for space applications. A characteristic of the Rankine cycle is that the working fluid (such as mercury) is condensed in the heat-rejection portion of the cycle. A condensing fluid such as mercury may exist in different flow regimes depending on whether or not the fluid is wetting or nonwetting. A study of the nature of the interface between liquid mercury and various solid surfaces in terms of interfacial electrical resistance and of wetting can be found in reference 1. For the nonwetting case the condensate on the tube surface is in the form of drops. For the wetting case the condensate forms a film on the tube surface. The flow differences under wetting and nonwetting conditions may influence the pressure distribution along the condensing tube, which, in turn, is important to the design of mercury condensers.

Nonwetting condensing data are discussed in references 2 to 6. Both nonwetting and "pseudowetting" (partial wetting) data were reported in reference 7. Mercury condensing pressure data in constant-diameter tubes under wetting conditions can be found in reference 8. Further experimental data of local and overall (from inlet to interface) pressure drop are needed to correlate the analytical methods of predicting frictional pressure drop for both wetted and nonwetted condensing. A part of the overall mercury condensing program initiated at NASA Lewis Research Center was the study of pressure drop under wetting and nonwetting condensing in tapered tubes. Particular emphasis in this study was given to the measurement of local static pressures from inlet to interface for condensing mercury in horizontal convectively cooled tubes. The test sections consisted of 4-foot-long tubes uniformly tapered from 0.50- to 0.20-inch nominal inside diameters. The vapor flow rates ranged from 0.025 to 0.052 pound per second corresponding to inlet velocities of 90 to 190 feet per second. The condensing lengths were varied between 18 to 45 inches for each flow rate. The secondary purpose of this investigation was to compare the measured local pressure gradients with the analytical predictions of Koestel (ref. 8) and Lockhart-Martinelli (ref. 9).

SYMBOLS

A cross-sectional area, ft^2

c_p specific heat of mercury vapor, Btu/(lb mass)(°F)

D tube outside diameter, ft

d tube inside diameter, ft

f friction factor, dimensionless

$\boldsymbol{f}$ function of

g_c conversion factor, 32.174 (lb mass)(ft)/(lb force)(sq sec)

h	local heat-transfer coefficient, Btu/(sec)(sq ft)($^{\circ}$F)
h_{fg}	mercury latent heat of vaporization, Btu/lb mass
k	thermal conductivity, Btu/(sec)(ft)($^{\circ}$F)
L	length, ft
l	distance from condensing tube inlet, ft
Nu	Nusselt number, dimensionless
P	pressure, lb/sq ft
PT	pressure transducer
q	local heat flux, Btu/(sec)(sq ft)
Re	Reynolds number, dimensionless
T	temperature, $^{\circ}$F
u	velocity, ft/sec
V	velocity ratio, u_{liq}/u_g, dimensionless
v	specific volume, cu ft/lb mass
We	Weber number, dimensionless
w	mass flow rate, lb mass/sec
x	quality, w_g/w_T, dimensionless
μ	viscosity, lb mass/(ft)(sec)
ρ	density, lb mass/cu ft
σ	surface tension, lb force/ft
Φ_g	Lockhart-Martinelli parameter, $\sqrt{(\Delta P/\Delta L)_{TPF}/(\Delta P/\Delta L)_g}$, dimensionless
X	two-phase flow modulus, $\sqrt{(\Delta P/\Delta L)_{liq}/(\Delta P/\Delta L)_g}$, dimensionless

Subscripts:

a	point at one pressure tap
b	point at downstream pressure tap
c	condensing

e	exit
g	mercury vapor
l	local
liq	liquid
N_2	nitrogen coolant
S	static
sat	saturated mercury vapor
sup	superheated mercury vapor
T	tube
TPF	two-phase frictional
t	tube
th	throat of venturi
tt	turbulent liquid and turbulent gas
vt	viscous liquid and turbulent gas
w	wall
O	inlet
1,8,20, 32,45	distance from condensing tube inlet, in.

Superscript:

—	average

APPARATUS

Experimental System and Components

The loop schematic and the components used in this investigation are presented in figures 1(a) and (b). Photographs of the experimental components are shown in figures 1(c) and (d). In general, the mercury loop consisted of an expulsion cylinder, a liquid flow measuring system, a preheater, a high heat-flux boiler, a main boiler, a vapor flow measuring venturi, a horizontal condensing tube, and a receiver for collecting the condensed mercury.

Approximately 160 pounds of triple-distilled mercury were stored in a stainless-steel expulsion cylinder. A calibrated orifice was located at the preheater inlet to measure liquid flow rate into the boiler.

4

Mercury
Gaseous argon
Gaseous nitrogen
Vacuum
Vacuum-pressure source mixture
Pressure transducer (differential)
Pressure transducer (absolute)

Image intensifier and
television movie camera

Mercury fill tube

Vent Solenoid valve Vent P_6 Mercury receiver Cooling manifolds Venturi T_g Manual shut-off valve

Pressure gage Mercury filter Condensing tube Expulsion cylinder

Mercury transfer cylinder

Solenoid valve

Boiler

High flux boiler

P_2

Orifice

Preheater

Pressure gage

Pres-sure gage

P_{45} P_{32} P_{20} P_8 P_1 P_5 P_4

Reference manifold

Solenoid valves

Solenoid valve

Manual shutoff valve

Solenoid valves

Compound pressure regulators

X-ray source

P_7

Vacuum pump

Manual control valve

Pressure regulator

Vent

Pressure regulator

Pres-sure gage

Cooling nitrogen supply

Manual shut-off valves

Solenoid valve

Compound pressure regulator

Cold trap

Pressure regulator

Pressure regulator

Argon supply

Manual shutoff valve

Pressure regulator

Solenoid valve

Pressure gages

(a) System schematic.

Figure 1. - Experimental system and components.

CD-8028
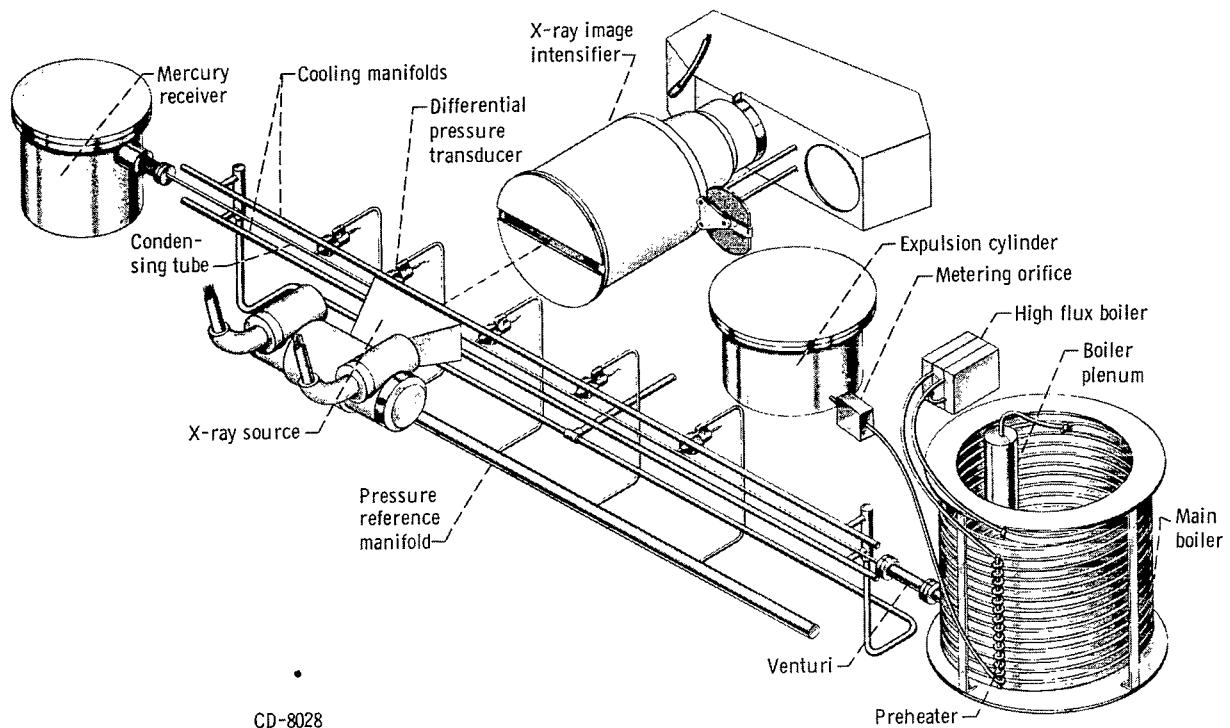
(b) Isometric drawing of components.

C-73728
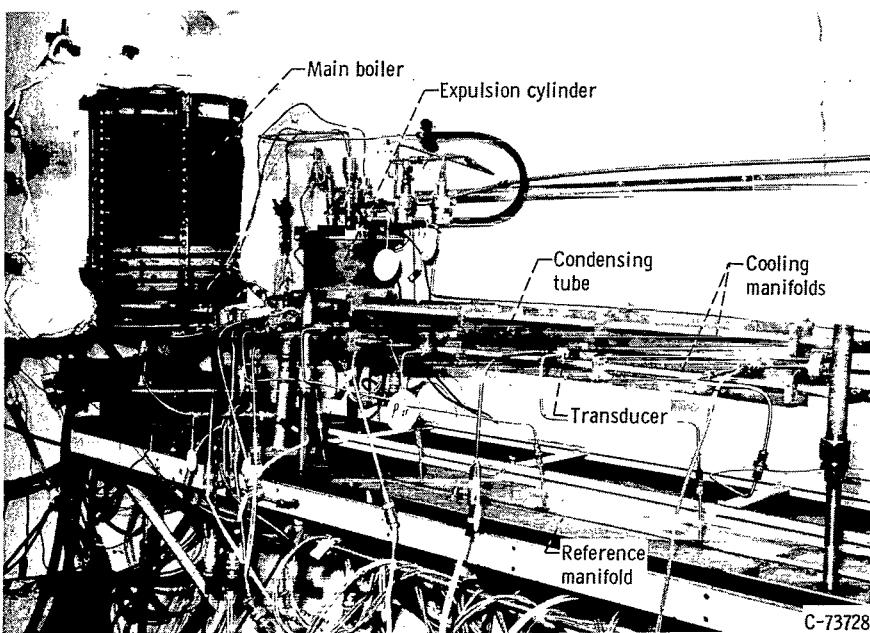
(c) Experimental components.
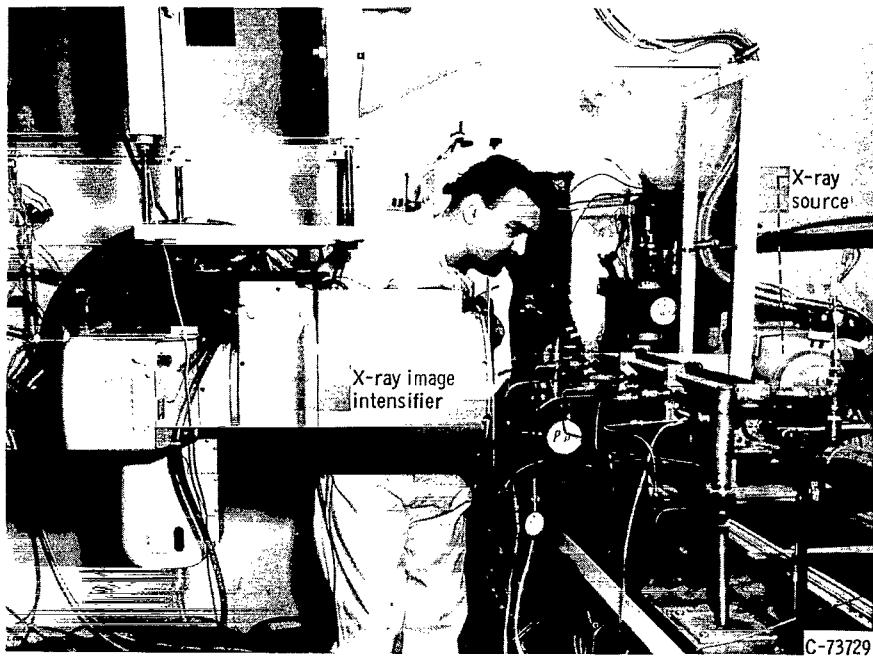
Figure 1. - Continued.

Boiling was accomplished in three stages. Mercury was first passed through the preheater, which raised the liquid temperature to the saturation point. This unit consisted of 4-foot coiled stainless-steel tube heated by a 1000-watt swaged nichrome wire. Nucleate boiling was accomplished in the high heat-flux unit consisting of stainless-steel tubing fitted into an electrically heated copper block. The operating power of this unit was approximately 2800 watts and the mercury quality at the exit of this unit was about 20 percent. The mixture was then passed into the main boiler, which supplied the heat needed to raise the quality into the 90 percent region. This unit was a resistance heater in which the power was applied directly to the tubing that formed the mercury flow passage. The mixture was then passed from the tubing into a plenum chamber, which was partially filled with stainless-steel cuttings to minimize liquid carryover. The average operating power of this unit was 8500 watts.

The flow of mercury vapor into the condensing tube was measured by a venturi having a throat diameter of 0.331 inch and an exit diameter of 0.460 inch. The test sections consisted of 4-foot-long tubes uniformly tapered from 0.50 to 0.20 inch nominal inside diameters (taper ratio of 0.075 in./ft). Copper tubes were used to obtain wetting data because mercury quickly wets copper. To obtain good experimental data, a short run time was required because of the high corrosion rate of mercury on copper. Because of the short run time needed to minimize the effect of tube wear, seven copper tubes (0.149-inch wall thickness) were used in this investigation. The nonwetting tests were conducted with a 0.035-inch-wall AISI 304 stainless-steel tube. Interface location was determined by an X-ray - image intensifier system. This system consisted of an X-ray source, an image intensifier, a television monitor, and a movie camera. A water-cooled heat exchanger was placed downstream of the condenser to ensure

complete condensation of mercury in case of system malfunction. The mercury receiver apparatus consisted of two stainless-steel cylinders connected in series. Receiver pressure was controlled by an argon pressure regulator.

The condenser was convectively cooled by gaseous nitrogen crossflow from two diametrically opposed manifolds having 0.052-inch holes spaced 3/8 inch apart. The nitrogen jet orifices in the cooling manifolds were approximately 1 inch from the centerline of the condensing tube.

Instrumentation

The location of pressure instrumentation on the test apparatus is shown in figure 1(a). Stainless-steel inductance-type pressure transducers, capable of operating in a mercury environment up to 900° F, were used to measure condenser pressures, inlet venturi static pressure, and venturi pressure drop. Differential pressure transducers used on the condenser tube were mounted with the high pressure sides to the tube and the low pressure sides referenced to a common nitrogen gas manifold. A 2-percent error can be expected in the output of the pressure transducers used in this investigation which corresponds to an error of 0.1 pound per square inch in the differential pressure. Static pressure taps were located at 1, 8, 20, 32, and 45 inches from the tube inlet. Each transducer in direct contact with mercury was mounted with the horizontal centerline of the diaphram on the centerline of the tube. Low-temperature transducers were used at all other locations in the system. The pressure data were recorded on a multichannel oscillograph.

Thermocouples throughout the system were constructed of the Instrument Society of America standard-calibration K Chromel-Alumel wires. A sheathed thermocouple was immersed in the mercury vapor stream at the venturi inlet. At other locations, bare thermocouples were spot welded to the outside surface of the various components such as the boiler, preheater, high heat-flux unit, etc. All temperatures were read out on self-balancing recording potentiometers.

PROCEDURE

Prior to each data run, a complete calibration of the absolute and differential pressure transducers was carried out. A complete listing of all pressure transducers and their respective calibration range is presented in table I. The transducers were calibrated with the coupling tube and transducer cavity filled with liquid mercury to simulate approximate test conditions. All differential pressure transducers on the condenser were calibrated simultaneously by pressurizing the mercury system with gaseous nitrogen through the venturi. The low pressure sides were all opened to atmospheric pressure, and a selected range of gage pressures was applied to the system. Desired oscillograph and readout gage spans were adjusted, and recorded runs were made over the calibration range so that transducer calibration curves could be plotted. The absolute pressure transducers were also calibrated simultaneously by applying pressure to the entire system. In order to zero these transducers, the system was first pumped to a vacuum (<1 torr). All other transducers in the system

were calibrated individually. Every high-temperature transducer was calibrated in the system at room temperature before each test run. For the high-temperature transducers in the vapor region the operating temperature of the diaphragms was estimated to be a maximum of approximately 300° F. The change in output caused by operating at these temperatures was approximately 0.5 percent of the maximum output of the transducers.

System operating procedure was identical for both nonwetting and wetting tests. Before initiating flow through the system, the mercury loop was evacuated to 0.18 torr, and the mercury heaters were brought to operating temperatures. Mercury flow through the system was initiated and maintained by pressurizing the top of the expulsion cylinder with regulated gaseous argon. The liquid flow rate was monitored according to observation of the pressure drop across the calibrated orifice located at the preheater inlet. Startup mass flow was set at 0.03 pound per second, and mercury vapor was allowed to purge the system for approximately 5 minutes to remove remaining noncondensables from the lines. After mercury vapor purging, the receiver pressure was increased gradually until the desired condenser inlet pressure for each weight flow was obtained. The gaseous nitrogen cooling flow was regulated to locate the interface 18 to 45 inches from the condenser inlet. The interface was observed with the X-ray image intensifier system. Data were recorded for vapor flow rates of 0.025 and 0.052 pound per second and for condenser inlet vapor temperatures corresponding to approximately 125° F superheat. Boiler performance tests indicated low quality for vapor saturation temperature at the boiler outlet. It was necessary in this system to raise the vapor temperature to 125° F superheat to minimize liquid carryover. Nominal test conditions were repeated on different days.

METHOD OF ANALYSIS

Two correlations for predicting pressure drops of flowing two-phase fluids in pipes are presently available. One correlation by Lockhart and Martinelli (ref. 9) is based on empirical data using adiabatic two-component fluids, while the other by Koestel (ref. 8) is based on a theoretical fog-flow model. Both of these correlations relate the ratio of the two-phase frictional pressure gradient to the pressure gradient of the vapor alone, where

$$\Phi_g^2 = \frac{\dfrac{\Delta P_{TPF}}{\Delta L}}{\dfrac{\Delta P_g}{\Delta L}} \tag{1}$$

To compare the experimental data with theory the two-phase frictional pressure gradient must be determined.

In the condensing process the static pressure drop is the sum of the frictional pressure drop and the pressure recovery (due to the momentum decrease). The frictional two-phase pressure drop between two pressure taps was determined by subtracting the calculated pressure recovery (due to momentum decrease) from the measured local static pressure difference. A force balance between two

pressure taps of a tapered tube can be expressed as

$$(P_a - P_b)_S \frac{A_{t,a} + A_{t,b}}{2} = -\frac{1}{g_c}(w_{g,a}u_{g,a} - w_{g,b}u_{g,b}$$

$$+ w_{liq,a}u_{liq,a} - w_{liq,b}u_{liq,b}) + F_{TPF} \qquad (2)$$

where F_{TPF} is the mean force due to friction within the element and the subscripts a and b refer to points at one pressure tap and the following downstream pressure tap, respectively. If liquid and vapor flow rates and the vapor velocity can be determined in equation (2), an assumption of either the liquid velocity or the velocity ratio is required to obtain the change in momentum within the increment. The velocity ratio V is defined as the ratio of the velocity of the liquid to that of the gas

$$V = \frac{u_{liq}}{u_g}$$

For high-velocity dropwise condensation (inlet vapor velocities on the order of 150 ft/sec) the drops that are entrained in the vapor stream are assumed to be accelerated very rapidly to approach a velocity ratio of one ($u_{liq} = u_g$). This assumption is based on the analytical predictions of velocity profiles of liquid drops being entrained into the vapor stream (ref. 8).

If a velocity ratio of one is assumed, the two-phase frictional pressure gradient between two pressure taps is given by the expression (see appendix A)

$$\left(\frac{\Delta P_{TPF}}{\Delta L}\right)_{a,b} = \frac{(P_a - P_b)_S \overline{A}_t - \frac{w_T^2}{\overline{\rho}g_c}\left(\frac{x_b}{A_{g,b}} - \frac{x_a}{A_{g,a}}\right)}{\int_{l_a}^{l_b} A_t dL} \qquad (3)$$

The quality at any point along the condensing tube must be established to determine the two-phase frictional pressure gradient. For saturated conditions at the inlet, the quality is related to the local heat flux q by the following expression:

$$x = x_0 - \frac{\int_0^l q\pi D dL}{w_T h_{fg}} \qquad (4)$$

But for the test conditions considered, approximately 125° F superheat existed at the inlet of the condenser, which amounts to an additional heat load of

10

2.5 percent. It is believed that a superheated vapor core existed with condensing on the tube surface. Observations based on unpublished photographic studies at the Lewis Research Center of nonwetting condensation in glass tubes indicated that condensing begins very near the tube inlet. Jakob (ref. 10) and Kutateladze (ref. 11) indicated that the entire mass of superheated vapor need not be cooled to the saturation temperature to initiate the condensation. It is further believed that the superheated vapor core is distributed along the entire condensing length. From the preceding considerations and by the use of equation (4) the quality with superheated conditions at any point along the condensing tube is related to the local heat flux q by the following expression

$$x = x_0 - \frac{\int_0^l q\pi D dL}{w_T[h_{fg} + c_p(T_{sup} - T_{sat})]} \tag{5}$$

By expressing the local heat flux in terms of the diameter and length, the quality at any point along the condensing tube is given by the following expression (see appendix B)

$$x = x_0 \left(1 - \frac{1.61\left\{\left[D_0 - (D_0 - D_e)\dfrac{l}{l_e}\right]^{1.805} - D_0^{1.805}\right\}}{1.805\left\{\left[D_0 - (D_0 - D_e)\dfrac{l_c}{l_e}\right]^{0.805} - D_0^{0.805}\right\}(D_0 + D_c)}\right) \tag{6}$$

By using equation (6), typical quality distributions as a function of length along the condensing tube can be calculated. These distributions are shown in figure 2(a). Knowing the quality along the condensing tube, the local vapor velocity u_g can be found by

$$u_g = \frac{w_T x}{\rho_g A_g} \tag{7}$$

where

$$A_g = \frac{A_t}{\dfrac{1-x}{x}\dfrac{\rho_g}{\rho_{liq}} + 1} \tag{8}$$

The superheated density ρ_g is determined from the superheated temperature and the saturated conditions of the mercury vapor (the superheated temperature was assumed constant along the condensing tube):

(a) Quality distribution.

(b) Axial velocity distribution.
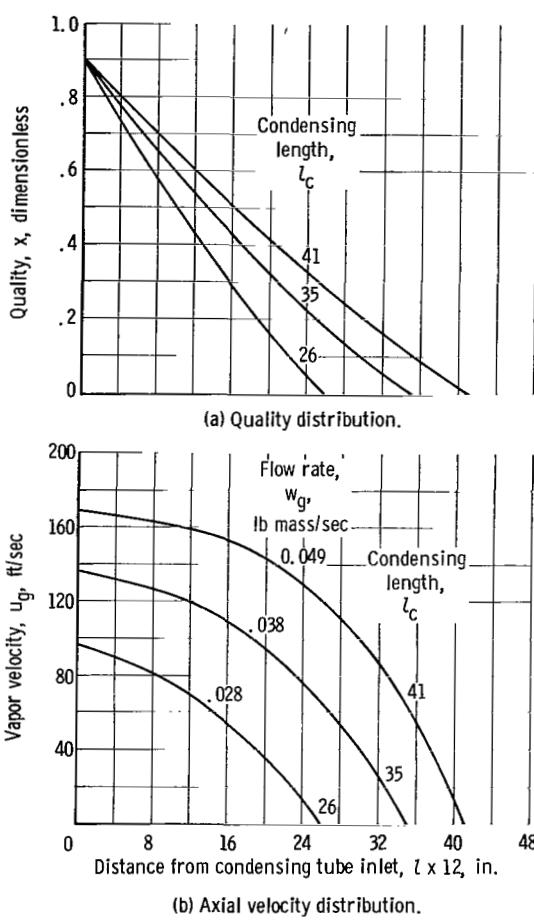
Figure 2. - Typical quality and axial velocity distributions along condensing tube for various condensing lengths (inlet quality, x_0, 0.90).

$$\rho_g = \rho_{sup} = \rho_{sat} \frac{T_{sat} + 460}{T_{sup} + 460} \qquad (9)$$

Typical velocity distributions along the condensing tube are shown in figure 2(b).

To calculate the Lockhart-Martinelli parameter, Φ_g, as defined in equation (1), the pressure gradient due to gas alone must be determined. By use of the Fanning equation, the mean one-phase frictional pressure gradient between two pressure taps is given by the following expression (see appendix A):

$$\left(\frac{\Delta P_g}{\Delta L}\right)_{a,b} = \frac{0.092 \ w_T^2}{\left(\frac{\pi}{4}\right)^2 g_c \overline{\rho} \ \overline{Re_g^{0.2}} \ \Delta L} \int_{l_a}^{l_b} \frac{x^2}{d^5} \, dL$$

$$(10)$$

EXPERIMENTAL RESULTS

The experimental static pressures for nonwetted and wetted flow are presented in tables II and III, respectively. The calculated flow rates of the mercury liquid entering the boiler, the vapor flow rate out of the boiler, and the tube inlet qualities are tabulated. The quality at the inlet of the condenser tube was calculated as the ratio of the vapor flow rate out of the boiler to the liquid flow rate into the boiler (see appendix D of ref. 6). Previous boiler performance tests indicated no liquid holdup in the boiler. The liquid flow rate was determined from the pressure drop across the calibrated orifice at the preheater inlet. The vapor flow rate was calculated from the standard equation for compressible flow through a venturi (ref. 12):

$$w_g = A_{th} KY \sqrt{2 g_c \rho_g \ \Delta P} \qquad (11)$$

where

A_{th} cross-sectional area of throat, ft^2

K experimentally determined flow coefficient, dimensionless

Y adiabatic expansion factor, dimensionless

(a) Vapor mass flow rate, 0.028 pound per second.

(b) Vapor mass flow rate, 0.038 pound per second.

(c) Vapor mass flow rate, 0.049 pound per second.
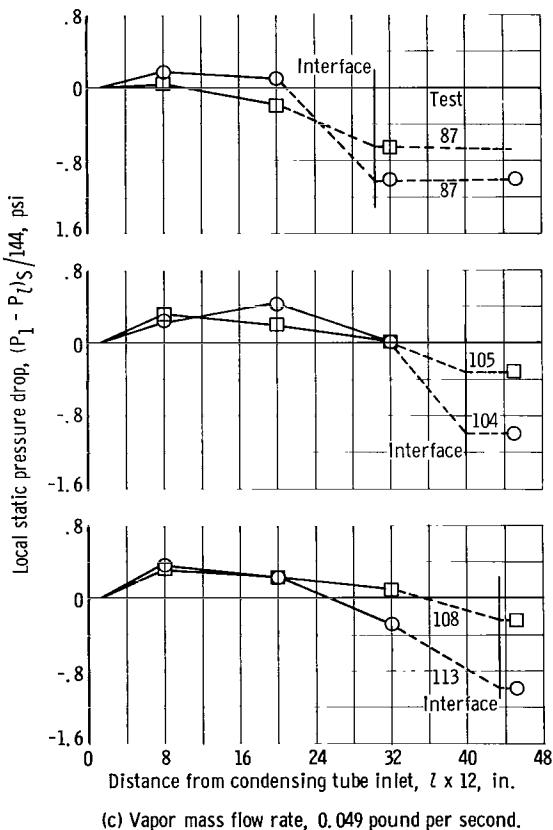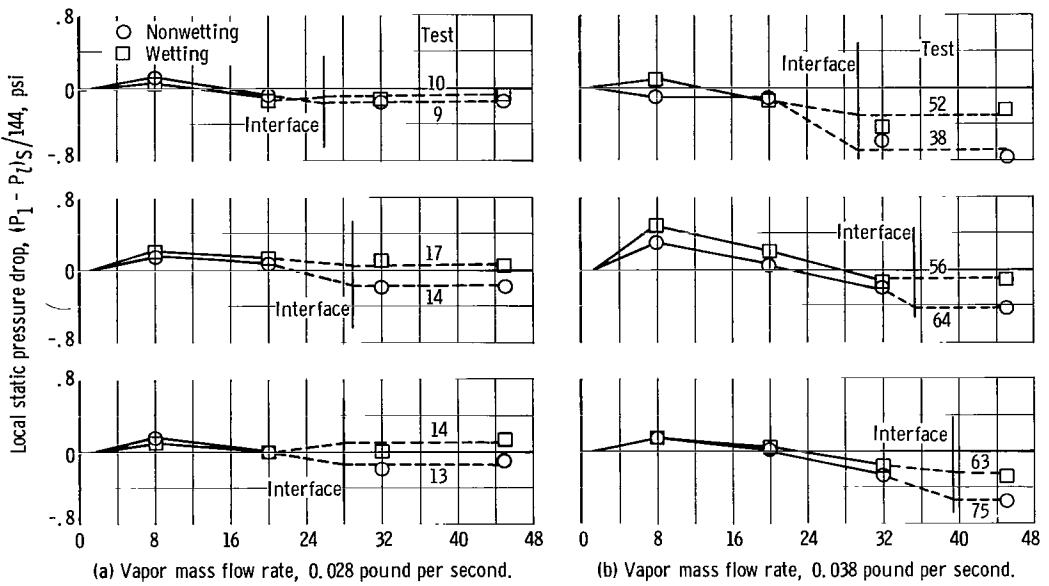
Figure 3. - Typical distributions of local static pressure drop for nonwetting and wetting conditions for three coolant flow rates.

← Flow direction
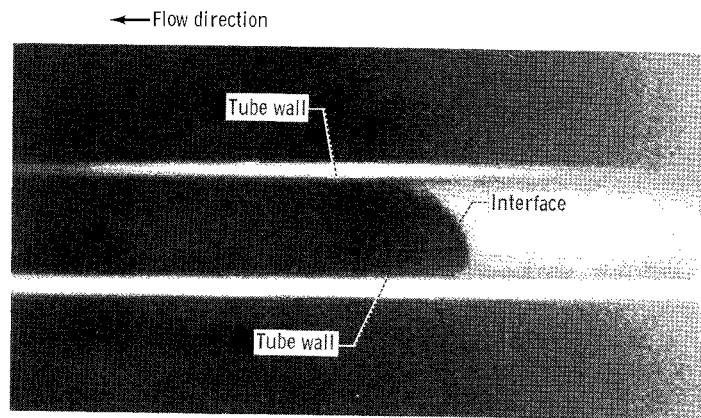
(a) Nonwetting in stainless-steel tube.
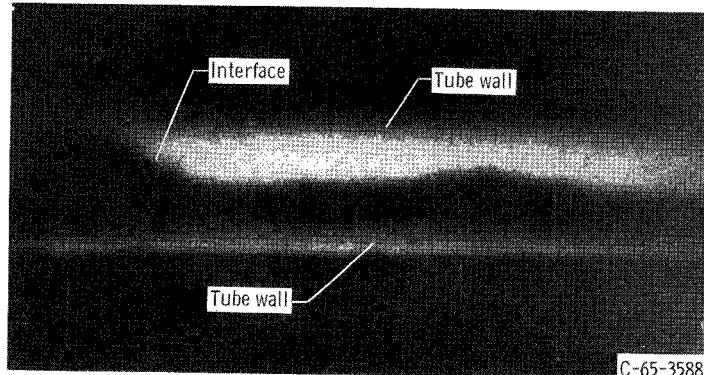
(b) Wetting in copper tube.

Figure 4. - Flow configurations at interface position for nonwetting and wetting flow of condensing mercury.

The density ρ_g was determined from the superheated temperature and the saturated conditions of the mercury vapor in the throat of the venturi. The measured static pressure drop ΔP from the inlet to the throat of the venturi was due to vapor only because the contribution of liquid carryover on the measured pressure drop at high vapor quality is small and can be neglected (see appendix D of ref. 6).

The majority of the wetted condensing data points presented in table III were obtained within an average run time of 30 minutes per tube. Because of the high corrosion rate of copper in the presence of mercury, the run time was kept to a minimum. After 30 minutes of mercury flow, there was a 5-percent average change in inside diameter for the upstream half of the copper tubes and a 3-percent average change in the downstream half. A comparison of repeated runs indicated that the small change in diameter of the copper tubes had negligible effect on the measured pressure drops. The inside diameters of the stainless-steel and copper tubes were the same at the beginning of the tests; thus the data obtained under wetting and nonwetting conditions were comparable.

DISCUSSION OF RESULTS

Measured Local Static Pressure Drop and Overall Pressure Difference

Typical distributions of local static pressure drop for various flow rates are presented in figure 3, (p. 13). These distributions were obtained from the difference between the measured static pressure at station 1 and the local static pressures along the condensing tube. The data presented for wetted and nonwetted conditions were obtained at approximately the same inlet flow conditions to the tube. Figures 3(b) and (c) indicate that the frictional pressure drop for wetted flow is slightly greater than that for the nonwetting condition. The higher frictional pressure drop occurs in the last half of the condensing length for the mass flow rates of 0.038 and 0.049 pound per second. During wetting condensation the liquid rolls down the side to the bottom of the tube (due to the influence of gravity), which results in liquid accumulation in the last half of the condensing length (fig. 4, p. 14). Observations of wetting condensation indicated that the buildup of liquid on the bottom of the tube was greater than the buildup of drops on the tube wall in nonwetting condensation. This liquid accumulation during wetting condensation decreases the effective vapor flow area, thereby increasing the vapor velocity, resulting in a higher frictional pressure drop. The above may not be true in a zero-gravity environment because of the difference in the liquid distribution in the tube.

The overall static pressure differences $(P_1 - P_{liq})_S$, obtained by substracting the average static pressure in the liquid from the static pressure at station 1, are presented in figures 5(a) and (b), respectively, for various flow rates under nonwetting and wetting conditions. The data indicate that the pressure rise due to a momentum decrease exceeds the pressure loss due to friction and droplet drag. Therefore, a net overall static pressure rise was obtained for both conditions at the weight flows and condensing lengths studied. The wetted and nonwetted overall static pressure differences are compared at three different flow rates at various condensing lengths in figure 5(c). At a mass flow rate of 0.028 pound per second, $(P_1 - P_{liq})_S$ was approximately equal for the wetted and nonwetted condensers. At mass flow rates of 0.038 and 0.049 pound per second, $(P_1 - P_{liq})_S$ for nonwetted flow exceeded that for wetted flow by a pressure rise of 0.3 and 0.6, respectively, at all condensing lengths considered. This pressure difference between nonwetted and wetted flows was significant compared with the overall pressure recovery.

Comparison of Experimental Data with Lockhart-Martinelli Correlation

Lockhart and Martinelli in reference 9 developed general correlations for calculating pressure drop in two-phase flow systems. They proposed the ratio of the two-phase frictional pressure gradient to the frictional pressure gradient of the gas alone, which is used to predict two-phase pressure drop:

$$\Phi_g^2 = \frac{\dfrac{\Delta P_{TPF}}{\Delta L}}{\dfrac{\Delta P_g}{\Delta L}} \tag{12}$$

(a) Nonwetting condition.

(b) Wetting condition.

(c) Comparison of nonwetting and wetting conditions.
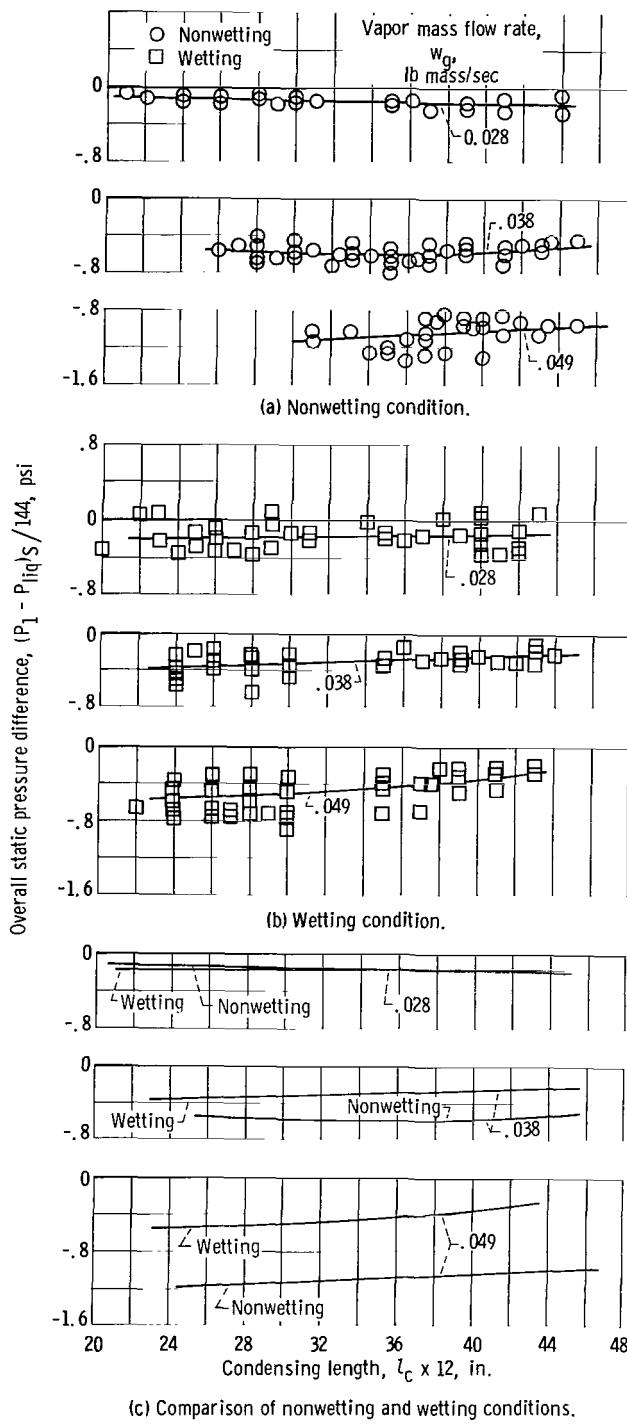
Figure 5. - Overall static pressure difference for various flow rates for nonwetting and wetting conditions.

Lockhart and Martinelli postulated that Φ_g is a function of the variable X, which is defined as

$$X^2 = \frac{\frac{\Delta P_{liq}}{\Delta L}}{\frac{\Delta P_g}{\Delta L}} \qquad (13)$$

The correlation of Φ_g and X was shown to exist and was defined by experimental data from reference 9.

The variable X (in eq. (13)) can be calculated from the fluid properties and the vapor and liquid mass flow rates. This ratio depends upon the flow mechanisms encountered. The frictional pressure drop data in this study were compared to two flow mechanisms: that is, viscous liquid-turbulent gas and turbulent liquid-turbulent gas where

$$X_{vt} = \left(\frac{16}{0.046} \frac{v_{liq}}{V_g} \frac{\mu_{liq}}{\mu_g} \frac{w_{liq}}{w_g}\right)^{0.5} Re_g^{-0.4}$$

$$(14)$$

$$X_{tt} = \left(\frac{w_{liq}}{w_g}\right)^{0.9} \left(\frac{v_{liq}}{v_g}\right)^{0.5} \left(\frac{\mu_{liq}}{\mu_g}\right)^{0.1}$$

$$(15)$$

To obtain the values of the Lockhart-Martinelli parameters, v_{liq} and μ_{liq} were determined at the saturation temperature based on the average pressure in the tube. The determination of v_g was based on the pressure and temperature of the superheated vapor. Because μ_g is a function of temperature only, it was based on a saturation temperature equal to the temperature of the superheated vapor. The saturation properties were obtained from reference 13.

(a) Nonwetting data.
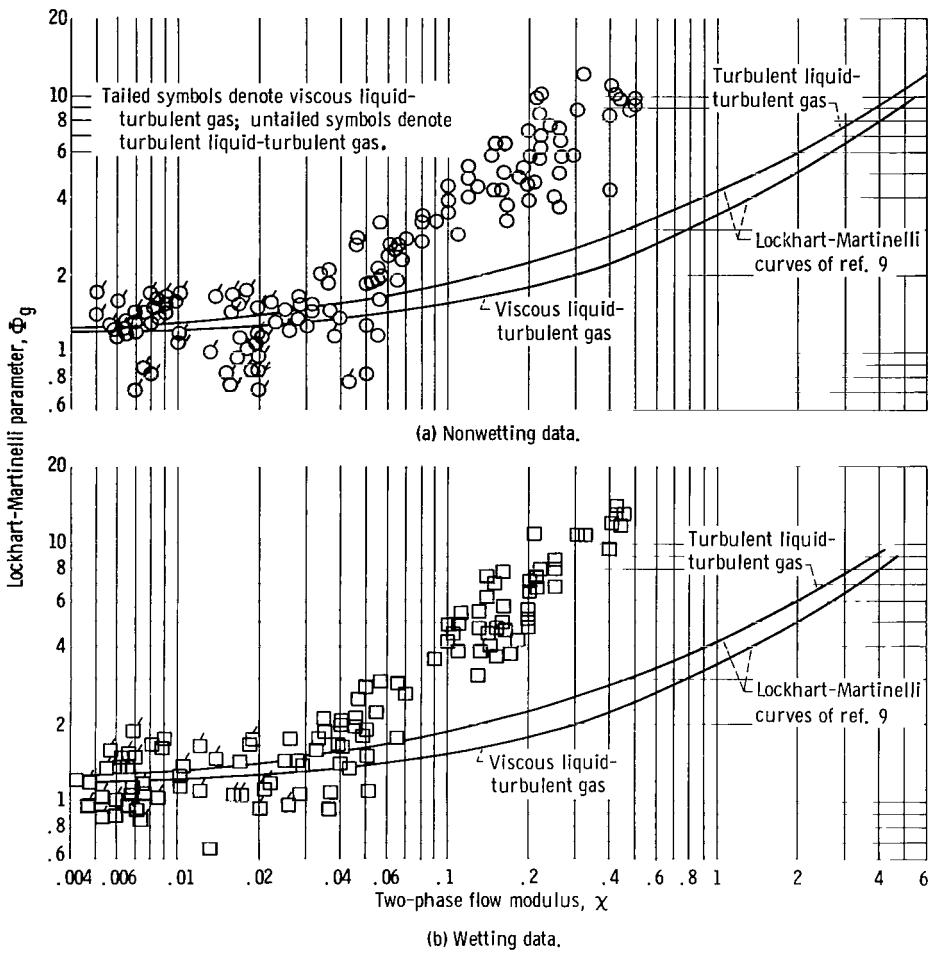
(b) Wetting data.

Figure 6. - Comparison of nonwetting and wetting data with Lockhart-Martinelli correlation.

A comparison of the Lockhart-Martinelli correlation with the experimental nonwetting and wetting data is presented in figures 6(a) and (b), respectively. The Lockhart-Martinelli correlation agreed with the data for qualities greater than 0.4 (i.e., corresponding to low values of the parameter X). For qualities less than 0.4 (i.e., corresponding to high values of the parameter X) the frictional pressure gradient was greater than that predicted by Lockhart and Martinelli. Examination of figures 6(a) and (b) indicated that the deviation increased with an increase in the parameter X. This deviation may result partly from the fact that flow regimes of mercury condensation are significantly different from the two-component, two-phase adiabatic flow model assumed by Lockhart and Martinelli. The nonwetting experiments of reference 5 and 8 on constant diameter tubes and the experiments of reference 6 on tapered tubes showed similar results.

Comparison of Experimental Data with the Fog-Flow Correlation

The fog-flow correlation of Koestel (ref. 8) treats the liquid and vapor

17

as a homogeneous flow and takes into account the buildup of drops on the inside tube wall. Under wetting conditions, drops are formed by the breakup of a thin film which forms on the condensing heat-transfer surface. The effective diameter through which the fog mixture flows is determined by the thickness of the drop layer.

Koestel (ref. 8) derived expressions that relate a fog-flow parameter $\Phi_g^2 x^{3/4}$ and the Weber number as functions of the ratio of tube diameter to fog-flow diameter:

$$We = \frac{d\rho_g u_g^2}{2g_c \sigma_{liq}} = \frac{0.371}{\left(\frac{d}{d_m}\right)^4 - \left(\frac{d}{d_m}\right)^3} \tag{16}$$

and

$$\Phi_g^2 x^{3/4} = \left(\frac{d}{d_m}\right)^{4.75} \tag{17}$$

where d_m is the diameter of the effective flow area remaining when condensed drops form on the wall. The theoretical relation between We and $\Phi_g^2 x^{3/4}$ can then be calculated by substituting a range of values of d/d_m in equations (16) and (17). Values of We and $\Phi_g^2 x^{3/4}$ were calculated from the experimental pressure measurements and the local mercury conditions in the tube.

Comparisons of the nonwetting and wetting data with the fog-flow correlation, presented in figures 7(a) and (b), show that for Weber numbers greater than 10 the fog-flow parameter $\Phi_g^2 x^{3/4}$ is independent of the Weber number. Thus Φ_g becomes a function of quality only. The fog-flow correlation agreed with the nonwetting and wetting data for qualities greater than 0.4 (i.e., corresponding to Weber numbers greater than 10) although considerable scatter existed. The scatter could be attributed to the small measured local static pressure differences along the condensing tube. The accuracies of these static pressure differences were limited by the accuracy of the pressure measurement. For example, a 2-percent error in one pressure pickup can result in a 30-percent change in the frictional pressure gradient in the low velocity region of the condensing tube. The fog-flow theory roughly predicted the trend of the nonwetting data for qualities less than 0.4 (i.e., corresponding to Weber numbers less than 10) although the frictional pressure gradients were slightly higher than those predicted by theory. The frictional pressure gradients for wetted flow were slightly higher than those for the nonwetted condition in the low quality region of the condensing tube (i.e., qualities less than 0.4). This difference may be due to the fact that the buildup of liquid on the bottom of the tube in wetting condensing was greater than the buildup of drops in nonwetting condensing.

SUMMARY OF RESULTS

An experimental study of the pressure drop of condensing mercury in con-

Theoretical (ref. 8)

(a) Nonwetting data.

Theoretical (ref. 8)

Fog-flow parameter, $\Phi_g^2 x^{3/4}$

20
10
8
6
4
2
1
.8
.6
.4

.06 .08 .1   .2   .4 .6 .8 1   2   4   6 8 10   20   40 60   100   200   400

Weber number, $dp_g u_g^2 / 2g_c \sigma_{liq}$
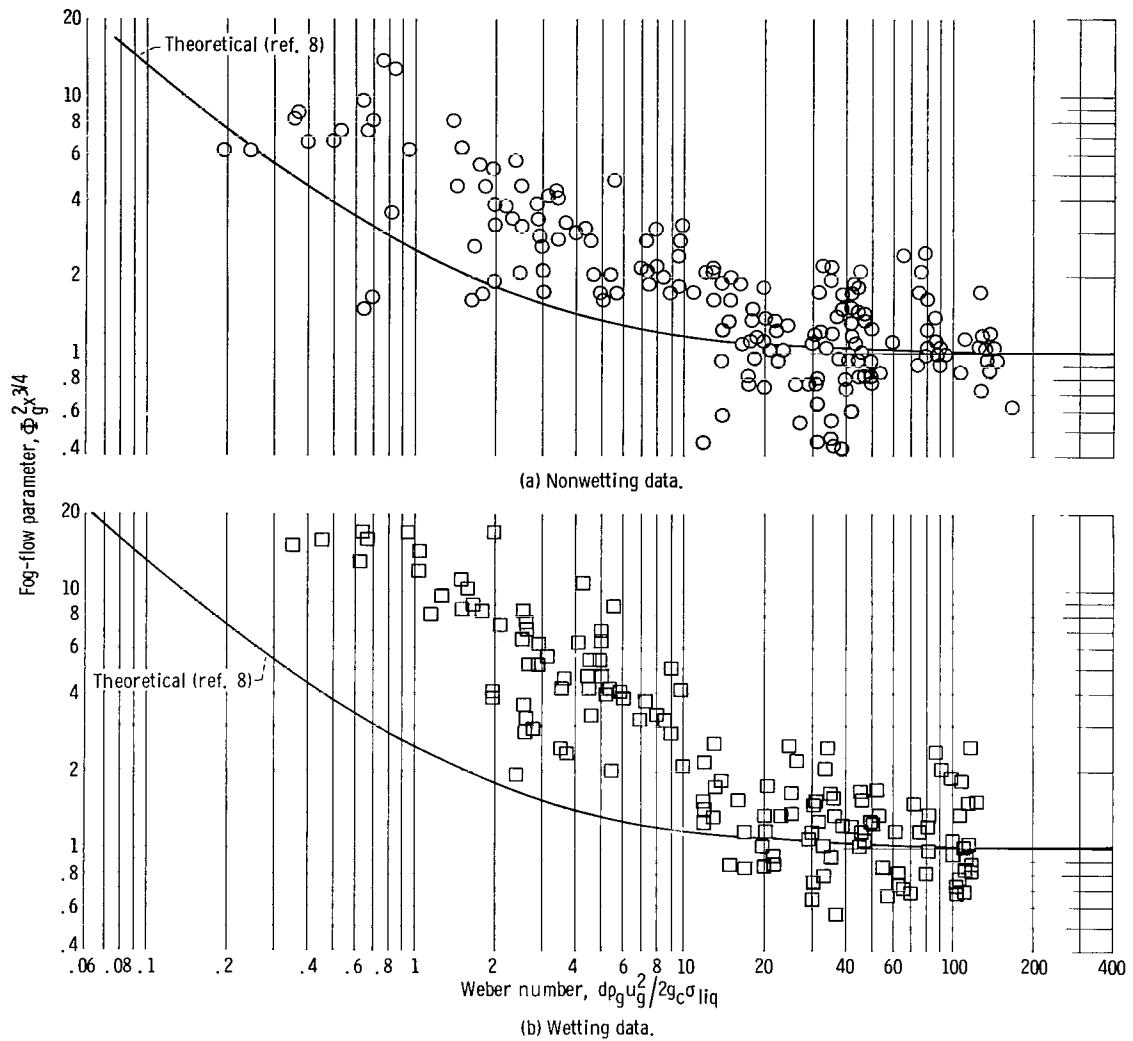
(b) Wetting data.

Figure 7. – Comparison of nonwetting and wetting data with fog-flow correlation.

vectively cooled tapered tubes under nonwetting and wetting conditions yielded the following results:

1. In general, an overall static pressure rise was obtained for both wetting and nonwetting conditions at the weight flows and condensing lengths considered because the pressure rise due to momentum decrease exceeded the pressure loss due to friction and droplet drag.

2. At a mass flow rate of 0.028 pound per second, the overall static pressure difference $(P_1 - P_{liq})_S$ was approximately equal for the wetted and nonwetted condensers. At mass flow rates of 0.038 and 0.049 pound per second, $(P_1 - P_{liq})_S$ for nonwetted flow exceeded that for wetted flow by a pressure rise of 0.3 and 0.6 pound per square inch, respectively, at all condensing lengths considered.

3. The Lockhart-Martinelli correlation agreed with the data for qualities greater than 0.4 (i.e., corresponding to low values of the parameter X). For qualities less than 0.4 (i.e., corresponding to high values of the parameter X) the frictional pressure gradients were greater than those predicted by Lockhart and Martinelli, and the deviation increased with an increase in the parameter X.

4. The fog-flow correlation of Koestel agreed with the nonwetted and wetted data for qualities greater than 0.4 (i.e., corresponding to Weber numbers greater than 10). The fog-flow theory roughly predicted the trend of the nonwetting data for qualities less than 0.4 (i.e., corresponding to Weber numbers less than 10) although the frictional pressure gradients were slightly higher than those predicted by theory. The frictional pressure gradients for wetted flow were slightly higher than those for the nonwetted condition in the low quality region of the condensing tube (last half of the condensing lengths). This difference may be due to the fact that the buildup of liquid on the bottom of the tube in wetting condensation was greater than the buildup of drops on the tube wall in nonwetting condensation.

Lewis Research Center,
National Aeronautics and Space Administration,
Cleveland, Ohio, November 8, 1965.

APPENDIX A

LOCAL PRESSURE GRADIENTS FOR TAPERED TUBE

When an element of a tapered tube (fig. 8) is considered, the sum of forces in the axial direction is

$$P_a A_{t,a} - \frac{(P_a + P_b)}{2} (A_{t,a} - A_{t,b}) - P_b A_{t,b} = -\frac{1}{g_c} (w_{g,a} u_{g,a} - w_{g,b} u_{g,b}$$
$$+ w_{liq,a} u_{liq,b} - w_{liq,b} u_{liq,b}) + F_{TPF} \qquad (A1)$$

where F_{TPF} is the mean force due to friction within the element. If a velocity ratio of one $(u_{g,a} = u_{liq,a}, u_{g,b} = u_{liq,b})$ is assumed, equation (A1) may be reduced to

$$(P_a - P_b)_S \left(\frac{A_{t,a} - A_{t,b}}{2}\right) = -\frac{1}{g_c} \left[(w_{g,a} + w_{liq,a}) u_{g,a} - (w_{g,b} + w_{liq,b}) u_{g,b}\right] + F_{TPF}$$

$$(A2)$$

But

$$w_T = w_g + w_{liq}$$

and

$$\bar{A}_t = \frac{(A_{t,a} + A_{t,b})}{2}$$

Then equation (A2) becomes

$$(P_a - P_b)_S \bar{A}_t = -\frac{w_T}{g_c} (u_{g,a} - u_{g,b}) + F_{TPF} \qquad (A3)$$

If the density changes are assumed small within the increment, the change in velocities becomes

$$u_{g,a} - u_{g,b} = \frac{w_T}{\bar{\rho}} \left(\frac{x_a}{A_{g,a}} - \frac{x_b}{A_{g,b}}\right)$$

$$(A4)$$

$P_a A_{t,a} x_a \qquad P_b A_{t,b} x_b$
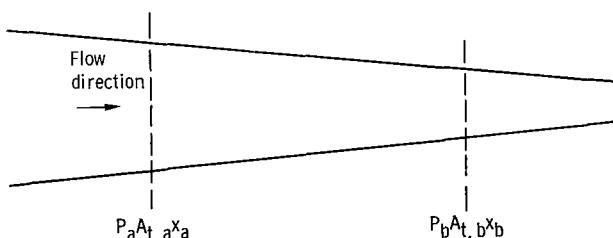
Figure 8. - Element of tapered tube.

where

$$\bar{\rho} = \frac{\rho_{g,a} + \rho_{g,b}}{2}$$

21

Substituting equation (A4) into equation (A3) and changing signs yield

$$(P_a - P_b)_S \overline{A}_t = \frac{w_T^2}{\overline{\rho} g_c} \left(\frac{x_b}{A_{g,b}} - \frac{x_a}{A_{g,a}} \right) + F_{TPF} \qquad (A5)$$

where

$$A_g = \frac{A_t}{\dfrac{1-x}{x} \dfrac{\rho_g}{\rho_{liq}} + 1}$$

and F_{TPF} is defined as

$$\frac{\Delta P_{TPF}}{\Delta L} \int_{l_a}^{l_b} A_t dL$$

Then solving for the two-phase frictional pressure gradient $\Delta P_{TPF}/\Delta L$ yields

$$\left(\frac{\Delta P_{TPF}}{\Delta L} \right)_{a,b} = \frac{(P_a - P_b)_S \overline{A}_t - \dfrac{w_T^2}{\overline{\rho} g_c} \left(\dfrac{x_b}{A_{g,b}} - \dfrac{x_a}{A_{g,a}} \right)}{\displaystyle\int_{l_a}^{l_b} A_t dL} \qquad (A6)$$

where the subscripts a and b refer to points at one pressure tap and the following downstream pressure tap, respectively.

The Fanning equation was used to determine the frictional pressure gradient due to gas alone:

$$\frac{\Delta P_g}{\Delta L} = \frac{4 f \rho_g u_g^2}{d 2 g_c} \qquad (A7)$$

where f is the friction factor for turbulent flow in a smooth tube and is expressed as (see ref. 14)

$$f = \frac{0.046}{Re_g^{0.2}} \qquad (A8)$$

and

$$u_g = \frac{4w_T x}{\pi \rho_g d^2} \qquad (A9)$$

Substituting equations (A8) and (A9) into equation (A7) and integrating to obtain a mean frictional pressure gradient from one pressure tap to the following pressure tap yield the following result

$$\left(\frac{\Delta P_g}{\Delta L}\right)_{a,b} = \frac{0.092\ w_T^2}{\left(\frac{\pi}{4}\right)^2 g_c \Delta L} \int_{l_a}^{l_b} \frac{x^2\, dL}{\rho_g Re_g^{0.2} d^5} \qquad (A10)$$

For small changes of Reynolds number and density between pressure taps the frictional pressure gradient due to gas alone becomes

$$\left(\frac{\Delta P_g}{\Delta L}\right)_{a,b} = \frac{0.092\ w_T^2}{\left(\frac{\pi}{4}\right)^2 g_c \overline{\rho}\ \overline{Re_g^{0.2}} \Delta L} \int_{l_a}^{l_b} \frac{x^2}{d^5}\, dL \qquad (A11)$$

where

$$\overline{Re_g^{0.2}} = \frac{\left(Re_g^{0.2}\right)_a + \left(Re_g^{0.2}\right)_b}{2}$$

The above integral was evaluated by numerical integration every inch along the tube length because the diameter and quality are now functions of length.

Equations (A6) and (A11) were used to determine the ratio of the two-phase frictional pressure gradient to the gas-phase pressure gradient, where

$$\left(\Phi_g^2\right)_{a,b} = \frac{\left(\dfrac{\Delta P_{TPF}}{\Delta L}\right)_{a,b}}{\left(\dfrac{\Delta P_g}{\Delta L}\right)_{a,b}} \qquad (A12)$$

APPENDIX B

QUALITY AS FUNCTION OF LENGTH FOR TAPERED TUBE

The quality at any point l along the condensing tube is related to the local heat flux q by the following expression:

$$x = x_O - \frac{\int_0^l q \pi D dL}{w_T[h_{fg} + c_p(T_{sup} - T_{sat})]} \tag{B1}$$

The heat flux at any point l along the tube is expressed as

$$q = (T_w - T_{N_2})h_{N_2} \tag{B2}$$

Assuming that the wall temperature and the coolant temperature are both nearly constant along the condensing length (small pressure changes), the average heat flux can be expressed as

$$\overline{q} = (T_w - T_{N_2})\overline{h_{N_2}} \tag{B3}$$

The cooling-gas-side heat-transfer coefficient is determined from Hilpert's equation for gas flowing perpendicular to cylinders (ref. 14)

$$Nu = B \, Re^n = B\left(\frac{\rho_{N_2} u_{N_2} D}{\mu_{N_2}}\right)^n \tag{B4}$$

where B and n are dimensionless constants depending on the value of Re. Assuming that the mass velocity $\rho_{N_2} u_{N_2}$ and μ_{N_2} of the nitrogen coolant are constant along the condensing tube yields

$$Nu = B'D^n = \frac{h_{N_2} D}{k_{N_2}}$$

where

$$B' = B\left(\frac{\rho_{N_2} u_{N_2}}{\mu_{N_2}}\right)^n \tag{B5}$$

Assuming k_{N_2} constant and solving for h_{N_2} give

$$h_{N_2} = \frac{B''D^n}{D} = B''D^{n-1}$$

where

$$B'' = k_{N_2}B' \tag{B6}$$

Similarly, the average cooling-side heat-transfer coefficient becomes

$$\overline{h_{N_2}} = B''\overline{D^{n-1}} = B'' \frac{1}{l_c} \int_0^{l_c} D^{n-1}dL \tag{B7}$$

From equations (B3) and (B7) the average heat flux obtained by integration can be expressed as

$$\overline{q} = (T_w - T_{N_2})B'' \frac{1}{l_c} \int_0^{l_c} D^{n-1}dL \tag{B8}$$

Dividing equation (B6) by (B7) results in

$$\frac{h_{N_2}}{\overline{h_{N_2}}} = \frac{l_c D^{n-1}}{\int_0^{l_c} D^{n-1}dL} \tag{B9}$$

and solving for h_{N_2} gives

$$h_{N_2} = \overline{h_{N_2}} \frac{l_c D^{n-1}}{\int_0^{l_c} D^{n-1}dL} \tag{B10}$$

Placing equation (B3) into equation (B10) yields the cooling-side heat-transfer coefficient:

$$h_{N_2} = \frac{\overline{q}}{T_w - T_{N_2}} \frac{l_c D^{n-1}}{\int_0^{l_c} D^{n-1}dL} \tag{B11}$$

The heat flux at any point along the tube is determined by equations (B2) and (B11):

$$q = \bar{q} \; \frac{l_c D^{n-1}}{\int_0^{l_c} D^{n-1} dL} \tag{B12}$$

The average heat flux can also be expressed as

$$q = \frac{w_T x_0 [h_{fg} + c_p (T_{sup} - T_{sat})]}{\pi \bar{D} l_c} \tag{B13}$$

where

$$\bar{D} = \frac{(D_0 + D_c)}{2}$$

Equating the average heat flux in equation (B13) to the average heat flux defined in equation (B8) and substituting equation (B13) into (B12) give the local heat flux:

$$q = \frac{w_T x_0 [h_{fg} + c_p (T_{sup} - T_{sat})] D^{n-1}}{\pi \bar{D} \int_0^{l_c} D^{n-1} dL} \tag{B14}$$

The quality can be expressed as a function of the diameter by placing equation (B14) into equation (B1) and simplifying:

$$x = x_0 \left(1 - \frac{\int_0^l D^n dL}{\int_0^{l_c} D^{n-1} dL} \right) \tag{B15}$$

Because the diameter varies linearly along the tube, it can be expressed as

$$D = C_1 + C_2 L \tag{B16}$$

Then the quality is expressed as a function of length

$$x = x_0 \left[1 - \frac{\int_0^l (C_1 + C_2 L)^n dL}{\bar{D} \int_0^{l_c} (C_1 + C_2 L)^{n-1} dL} \right] \tag{B17}$$

26

From table of integrals

$$\int (a + bx)^c \, dx = \frac{(a + bx)^{c+1}}{(c + 1)b}$$

Then

$$x = x_0 \left\{ 1 - \frac{\left. \dfrac{(C_1 + C_2 L)^{n+1}}{(n + 1)C_2} \right]_0^{l}}{\overline{D}\left[\dfrac{(C_1 + C_2 L)^{n}}{nC_2} \right]_0^{l_c}} \right\} \qquad (B18)$$

By putting in the limits of integration, equation (B18) is expressed as

$$x = x_0 \left\{ 1 - \frac{\left[\dfrac{(C_1 + C_2 l)^{n+1} - C_1^{n+1}}{(n + 1)C_2} \right]}{\overline{D}\left[\dfrac{(C_1 + C_2 l_c)^{n} - C_1^{n}}{nC_2} \right]} \right\} \qquad (B19)$$

where

$$C_1 = D_0 \qquad (B20a)$$

$$C_2 = - \frac{(D_0 - D_e)}{l_e} \qquad (B20b)$$

$$\overline{D} = \frac{(D_0 + D_c)}{2} \qquad (B20c)$$

Substituting equation (B20) into equation (B19) yields the following:

$$x = x_0 \left(1 - \frac{2n\left\{ \left[D_0 - (D_0 - D_e)\dfrac{l}{l_e} \right]^{n+1} - D_0^{n+1} \right\}}{(n + 1)\left\{ \left[D_0 - (D_0 - D_e)\dfrac{l_c}{l_e} \right]^{n} - D_0^{n} \right\}(D_0 + D_c)} \right) \qquad (B21)$$

The exponent n can be determined from the average Nusselt number for the condensing tube, where

27
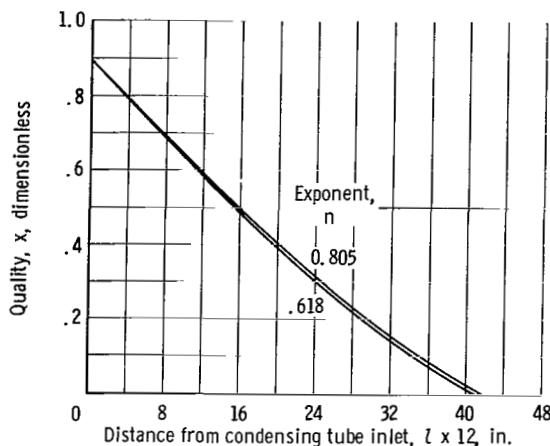
Figure 9. - Quality distributions along condensing tube for exponent n of 0.805 and 0.618 (inlet quality, x_0, 0.90).

$$\overline{Nu} = \frac{\overline{h_{N_2}}\overline{D}}{\overline{k_{N_2}}} \tag{B22}$$

From equations (B3) and (B13) the average cooling heat-transfer coefficient for a given flow rate and condensing length is expressed as

$$\overline{h_{N_2}} = \frac{w_T x_0 [h_{fg} + c_p(T_{sup} - T_{sat})]}{\pi \overline{D} l_c (T_w - T_{N_2})} \tag{B23}$$

Then

$$\overline{Nu} = \frac{w_T x_0 [h_{fg} + c_p(T_{sup} - T_{sat})]}{\pi l_c k_{N_2} (T_w - T_{N_2})} \tag{B24}$$

For the flow rates and condensing lengths considered the average Nusselt number varied from approximately 90 to 260.

From reference 14 the exponent n in equation (B21) is equal to the following values: n = 0.618 where Nu = 29.5 to 121; n = 0.805 where Nu = 121 to 528. The difference in the variation of quality against length for an exponent n of 0.618 and 0.805 is negligible (see fig. 9).

Assuming a value of n = 0.805 the distribution of quality can be determined from equation (B21):

$$x = x_0 \left(1 - \frac{1.61\left\{\left[D_0 - (D_0 - D_e)\dfrac{l}{l_e}\right]^{1.805} - D_0^{1.805}\right\}}{1.805\left\{\left[D_0 - (D_0 - D_e)\dfrac{l_c}{l_e}\right]^{0.805} - D_0^{0.805}\right\}(D_0 + D_c)} \right) \tag{B25}$$

REFERENCES

1. Droher, Joseph J.: Studies of Interfacial Effects Between Mercury and Steel. Rept. No. ORO-69, AEC, 1952.

2. Hays, Lance: Investigation of Condensers Applicable to Space Power Systems. Pt. I. Direct Condensers. Rept. No. 1588, Electro-Optical Systems, Inc., Aug. 15, 1962.

3. Kiraly, R. J.; and Koestel, Alfred: The SNAP-2 Power Conversion System Topical Rept. No. 8, Mercury Condensing Research Studies. Rept. No. ER-4442, Thompson Ramo Wooldridge, Inc. May 31, 1961

4. Jaenke, C. T.; Koestel, Alfred; and Reitz, John G.: The SNAP-2 Power Conversion System. Orbital Force Field Boiling and Condensing Experiments (Offbace). Topical Rept. No. 13, Rept. No. ER-4670, Thompson Ramo Wooldridge, Inc., Oct. 1962.

5. Albers James A.; and Macosko, Robert P.: Experimental Pressure-Drop Investigation of Nonwetting, Condensing Flow of Mercury Vapor in a Constant Diameter Tube in a 1-G and Zero-Gravity Environments. NASA TN D-2838, 1965.

6. Albers, James A. and Macosko, Robert P.: Condensation Pressure Drop of Nonwetting Mercury in a Uniformly Tapered Tube in 1-g and Zero-Gravity Environments. NASA TN D-3185, 1965.

7. Gido, R. G.; and Koestel, Alfred: Mercury Wetting and Nonwetting Condensing Research. Rept. No. ER-5214, Thompson Ramo Wooldridge, Inc., Jan. 1963.

8. Koestel, Alfred; Gutstein, Martin U.; and Wainwright, Robert T.: Study of Wetting and Nonwetting Mercury Condensing Pressure Drops. NASA TN D-2514, 1964.

9. Lockhart, R. W.; and Martinelli, R. C.: Proposed Correlation of Data for Isothermal Two-Phase Two-Component Flow in Pipes. Chem. Eng. Prog., vol. 45, no. 1, 1949, pp. 39-48.

10. Jakob, Max: Heat Transfer in Evaporation and Condensation, II. Mech. Eng., vol. 58, no. 11, Nov. 1936, pp. 729-739.

11. Kutateladze, S. S. (S. J. Rimshaw, Trans.): Heat Transfer in Condensation and Boiling. Rept. No. TR-3770, AEC, 1952, pp. 53-60.

12. Anon.: Power Test Codes-Instruments and Apparatus. ASME, 1959, pt. 5, ch.4.

13. Wetherford, W. D., Jr.; Tyler, J. C.; and Ku, P. M.: Properties of Inorganic Energy-Conversion and Heat-Transfer Fluids for Space Applications Rept. No. 61-96, WADD, Nov. 1961.

14. McAdams, W. H.: Heat Transmission. Third ed., McGraw-Hill Book Co., Inc., 1954.

TABLE I. - TRANSDUCER CALIBRATION RANGE

Pressure transducer	Description	Calibration range, psi	Temperature region
PT_2	Pressure drop across orifice	[a]0 to 60	Low
PT_4	Venturi inlet pressure	[b]0 to 24	High
PT_5	Venturi pressure drop	[a]0 to 4	High
PT_6	Mercury receiver pressure	[b]0 to 24	Low
PT_7	Reference manifold pressure	[b]0 to 24	Low
PT_1	Pressure 1 in. from condensing tube inlet	[a]0 to 4	High
PT_8	Pressure 8 in. from condensing tube inlet	[a]0 to 4	
PT_{20}	Pressure 20 in. from condensing tube inlet	[a]0 to 4	
PT_{32}	Pressure 32 in. from condensing tube inlet	[a]0 to 4	
PT_{45}	Pressure 45 in. from condensing tube inlet	[a]0 to 4	↓

[a]Differential.

[b]Absolute.

TABLE II. - EXPERIMENTAL NONWETTING DATA

Point identi-fication	Total mass flow rate, w_T, lb/sec	Vapor mass flow rate, w_g, lb/sec	Inlet quality, x_0	Inlet temper-ature, T_g, °F	1	8	20	32	45	Condens-ing length, $l_c \times 12$, in.
					Static pressure, $P_S/144$, psia					
1	0.0311	0.0285	0.92	845	14.5	14.5	14.6	14.6	14.6	18
2	.0306	.0284	.93	865	14.5	14.4	14.0	14.5	14.5	21
3	.0310	.0265	.86	850	14.2	14.2	14.3	14.4	14.4	22
4	.0306	.0283	.92	860	14.2	14.2	14.3	14.4	14.4	24
5	.0310	.0289	.93	850	14.3	14.4	14.5	14.5	14.5	24
6	.0312	.0275	.88	860	14.4	14.2	14.6	14.4	14.4	24
7	.0306	.0279	.91	860	14.5	14.4	14.6	14.6	14.6	26
8	.0312	.0273	.88	865	14.6	14.4	14.6	14.6	14.6	26
9	.0311	.0291	.94	870	14.4	14.3	14.4	14.6	14.6	26
10	.318	.0285	.90	865	14.6	14.4	14.6	14.7	14.7	27
11	.0306	.0288	.94	860	14.5	14.4	14.5	14.6	14.6	28
12	.0318	.0297	.94	860	14.5	14.4	14.5	14.7	14.6	28
13	.0312	.0263	.84	860	14.2	14.1	14.3	14.4	14.4	29
14	.0315	.0270	.86	845	14.4	14.2	14.3	14.6	14.6	29
15	.0308	.0289	.94	850	14.4	14.3	14.4	14.4	14.6	30
16	.0312	.0256	.82	865	14.0	13.9	13.9	14.1	14.2	30
17	.0308	.0289	.94	850	14.4	14.4	14.4	14.6	14.6	30
18	.0316	.0294	.93	875	14.4	14.4	14.5	14.7	14.6	30
19	.0312	.0250	.80	870	14.2	14.1	14.0	14.4	14.4	30
20	.0314	.0291	.93	880	14.4	14.2	14.2	14.3	14.5	35
21	.0308	.0278	.90	865	14.5	14.3	14.3	14.4	14.6	35
22	.0315	.0274	.90	850	14.5	14.3	14.4	14.5	14.6	35
23	.0312	.0291	.93	880	14.3	14.1	14.2	14.2	14.4	36
24	.0308	.0286	.93	860	14.3	14.3	14.3	14.3	14.5	37
25	.0312	.0262	.84	865	14.2	14.1	14.2	14.2	14.5	37
26	.0314	.0289	.92	880	14.5	14.4	14.3	14.4	14.6	39
27	.0312	.0262	.84	865	14.4	14.2	14.2	14.4	14.6	39
28	.0312	.0248	.86	870	14.2	14.2	14.0	14.2	14.5	43
29	.0312	.0287	.92	880	14.4	14.3	14.2	14.3	14.5	43
30	.0314	.0287	.91	880	14.4	14.2	14.2	14.3	14.5	41
31	.0312	.0265	.85	865	14.6	14.4	14.4	14.6	14.8	41
32	.0410	.0375	.92	855	14.5	14.4	14.6	15.1	15.1	26
33	.0415	.0399	.96	820	14.4	14.1	14.4	14.8	14.9	27
34	.0415	.0389	.94	825	14.4	14.0	14.4	14.8	14.8	28
35	.0410	.0370	.90	850	14.6	14.4	14.6	15.0	15.0	28
36	.0435	.0366	.86	850	14.2	14.0	14.2	14.8	14.8	28
37	.0420	.0377	.90	875	14.2	14.0	14.2	14.3	14.8	28
38	.0400	.0367	.92	865	14.5	14.6	14.6	15.1	15.3	29
39	.0378	.0319	.84	805	15.2	15.0	15.2	15.4	15.5	30
40	.0420	.0398	.95	825	14.2	13.8	14.1	14.6	14.7	30
41	.0410	.0370	.90	855	14.4	14.2	14.3	14.3	14.3	30
42	.0403	.0390	.97	830	14.4	14.2	14.6	15.0	15.0	↓
43	.0405	.0399	.98	835	14.4	14.4	14.7	15.2	15.3	
44	.0410	.0360	.88	865	14.4	14.4	14.4	15.0	15.0	
45	.0435	.0365	.86	865	14.0	13.7	13.9	14.6	14.6	
46	.0415	.0389	.94	855	14.3	14.1	14.2	14.9	14.9	30
47	.0420	.0376	.90	885	14.2	14.0	14.1	14.8	14.8	30
48	.0420	.0381	.91	850	14.4	14.2	14.4	15.0	15.0	31
49	.0400	.0354	.69	865	14.1	14.1	14.0	14.6	14.8	32
50	.0415	.0392	.94	820	14.2	13.8	13.9	14.1	14.7	33
51	.0425	.0369	.87	875	13.3	13.6	13.6	14.0	14.6	33
52	.0412	.0382	.93	845	14.3	14.2	14.1	14.4	14.8	33
53	.0450	.0360	.80	755	14.3	14.0	14.0	14.3	14.9	33
54	.0410	.0398	.97	840	14.6	14.4	14.6	14.9	15.3	34
55	.0415	.0376	.91	860	14.5	14.2	14.3	14.6	15.2	34
56	.0407	.0401	.99	805	14.2	13.8	13.8	14.0	14.7	35
57	.0405	.0367	.91	840	14.2	14.0	13.9	14.2	14.7	↓
58	.0420	.0383	.91	860	14.4	14.1	14.2	14.6	15.0	
59	.0430	.0369	.86	880	13.9	13.6	13.7	14.0	14.6	
60	0.0415	0.0374	0.90	860	14.3	14.2	14.4	14.5	14.8	35
61	.0413	.0388	.94	895	14.2	14.0	15.0	15.2	15.9	↓
62	.0400	.0369	.92	870	14.6	14.6	14.4	14.7	15.4	
63	.0390	.0344	.88	815	14.9	14.7	14.9	15.1	15.4	
64	.0391	.0337	.86	795	14.9	14.6	14.9	15.1	15.4	↓
65	.0415	.0390	.94	850	14.5	14.3	14.5	15.2	15.2	36
66	.0400	.0396	.99	855	14.5	14.3	14.5	15.3	15.2	36
67	.0430	.0388	.90	845	14.2	13.8	13.8	13.9	14.7	37
68	.0418	.0415	.99	830	14.4	14.0	14.1	14.2	15.0	37
69	.0430	.0348	.81	885	14.0	13.7	13.8	13.8	14.7	37
70	.0392	.0386	.96	830	14.2	14.0	13.9	14.1	14.8	37
71	.0415	.0376	.91	815	14.3	14.0	14.0	14.2	14.9	37
72	.0442	.0387	.87	750	14.0	13.7	13.8	14.0	14.6	38
73	.0380	.0348	.92	815	15.0	14.8	15.0	15.3	15.6	38
74	.0415	.0396	.95	835	14.4	14.0	14.0	14.1	14.9	39
75	.0425	.0371	.87	850	14.0	14.2	14.4	14.7		39
76	.0433	.0366	.84	890	14.1	13.7	13.8	13.9	14.1	↓
77	.0413	.0369	.89	930	14.1	13.8	13.7	13.8	14.7	
78	.0425	.0376	.88	770	14.3	14.1	14.0	14.2	14.9	
79	.0425	.0381	.89	845	14.2	14.1	14.2	14.5	14.8	↓
80	.0430	.0389	.90	855	14.3	13.9	13.8	13.8	14.8	41
81	.0417	.0380	.91	920	14.3	14.0	13.9	13.8	15.0	41
82	.0408	.0347	.85	790	14.9	14.5	14.7	15.0	15.3	42
83	.0430	.0368	.90	860	14.3	13.9	13.8	13.7	14.8	43
84	.0430	.0384	.89	825	14.2	14.0	14.1	14.4	14.7	43
85	.0410	.0400	.97	845	14.8	14.1	14.1	14.3	15.2	43
86	.0417	.0404	.97	915	14.0	13.7	13.5	13.5	14.6	43
87	.0520	.0489	.94	705	14.6	14.4	14.5	15.6	15.6	31
88	.0510	.0470	.92	720	14.3	14.1	14.0	15.4	15.5	31
89	.0510	.0478	.94	850	13.7	13.3	13.4	14.3	15.0	33
90	.0520	.0480	.92	710	14.3	14.0	14.0	14.5	15.4	33
91	.0520	.0486	.94	805	14.0	13.7	13.8	14.3	15.3	34
92	.0505	.0469	.93	860	13.7	13.3	13.3	13.6	15.0	35
93	.0502	.0491	.98	870	15.3	15.3	15.1	15.7	16.5	35
94	.0505	.0500	.99	860	14.5	14.4	14.3	15.0	16.1	36
95	.0520	.0503	.97	865	17.3	17.0	16.8	17.4	18.4	36
96	.0525	.0483	.92	845	14.1	13.9	13.8	14.2	15.0	37
97	.0520	.0510	.98	860	15.3	15.2	16.9	17.4	18.4	37
98	.0520	.0504	.92	835	13.8	13.6	13.4	14.0	14.8	37
99	.0515	.0491	.95	865	13.7	13.3	13.2	13.4	15.0	37
100	.0505	.0475	.94	840	13.7	13.5	13.3	13.9	14.8	37
101	.0523	.0487	.93	840	14.1	13.8	13.7	14.1	14.9	38
102	.0510	.0506	.99	875	17.2	17.0	16.7	17.1	18.3	38
103	.0520	.0503	.97	860	17.7	16.9	16.7	17.2	18.2	38
104	.0520	.0510	.98	855	17.2	17.0	16.8	17.2	18.2	39
105	.0500	.0490	.98	880	15.5	15.5	15.2	15.7	16.5	39
106	.0510	.0510	.98	880	17.0	16.8	16.4	16.7	18.1	40
107	.0512	.0451	.88	715	13.9	13.5	13.5	13.8	15.2	40
108	.0505	.0490	.97	845	14.3	14.0	13.7	14.1	15.3	40
109	.0508	.0450	.88	755	14.6	14.2	14.4	15.0	15.5	41
110	.0530	.0490	.92	860	14.9	14.7	13.9	14.7	15.9	41
111	.0510	.0490	.96	885	14.4	14.1	14.1	15.0	15.4	42
112	.0520	.0498	.96	850	17.3	17.0	16.6	16.9	18.4	43
113	.0501	.0475	.97	780	15.1	14.7	14.8	15.4	16.1	44
114	.0520	.0510	.98	845	13.8	13.6	13.2	13.5	14.8	45

TABLE III. - EXPERIMENTAL WETTING DATA

Point identi-fication	Liquid mass flow rate, w_T, lb/sec	Vapor mass flow rate, w_g, lb/sec	Inlet quality, x_o	Inlet temper-ature, T_g, °F	1	8	20	32	45	Condensing length, $l_c \times 12$, in.
					Static pressure, $P_S/144$, psia					
1	0.0310	0.0280	0.90	820	15.2	15.1	15.1	15.2	15.1	18
2	.0313	.0265	.85	850	17.4	17.4	17.4	----	17.7	20
3	.0318	.0280	.88	820	15.2	15.1	15.1	15.2	15.0	22
4	.0322	.0310	.96	825	17.3	17.1	17.2	17.3	17.6	23
5	.0315	.0275	.87	820	15.3	15.1	15.2	15.2	15.1	24
6	.0313	.0244	.75	850	17.4	17.4	17.4	----	17.7	24
7	.0310	.0300	.97	845	17.2	17.4	17.5	17.5	----	25
8	.0300	.0276	.92	855	17.5	17.4	17.4	----	17.7	25
9	.0318	.030	.96	840	17.4	17.4	17.5	17.4	----	26
10	.0322	.029	.92	820	14.2	14.1	14.3	14.3	14.2	26
11	.0320	.031	.98	820	17.6	17.3	17.5	17.5	17.8	26
12	.0312	.0253	.81	860	17.3	17.4	17.3	----	17.7	26
13	.0315	.0272	.86	860	17.4	17.3	17.3	----	17.7	27
14	.0320	.0266	.82	820	14.3	14.2	14.3	14.3	14.2	28
15	.0310	.0266	.86	860	17.4	17.4	17.3	----	17.7	28
16	.030	.029	.97	845	17.5	17.4	17.5	17.5	----	29
17	.0313	.0283	.90	820	15.4	15.2	15.3	15.3	15.3	29
18	.0318	.0305	.97	820	17.7	17.5	17.6	16.7	16.9	29
19	.032	.0264	.82	865	17.3	17.3	17.2	---	17.6	29
20	.0318	.0295	.92	845	17.3	17.3	17.4	17.4	----	30
21	.0326	.0281	.86	850	14.2	14.1	14.3	14.4	14.3	30
22	.0303	.0303	1.00	800	14.3	14.2	14.3	14.5	14.4	31
23	.0312	.0266	.85	860	17.3	17.3	17.3	----	17.5	31
24	.0310	.0297	.83	850	14.6	14.5	14.6	14.7	14.6	34
25	.0322	.0315	.98	845	17.6	17.1	17.4	17.1	17.4	35
26	.0313	.0282	.90	820	15.6	15.3	15.4	15.7	15.8	35
27	.0307	.0272	.88	870	17.5	17.0	16.9	----	17.7	36
28	.0310	.0262	.84	865	17.4	17.3	17.3	----	17.6	37
29	.0315	.0285	.90	820	15.8	15.5	15.5	15.8	15.7	38
30	.0322	.0294	.91	850	14.8	14.6	14.8	14.8	14.8	38
31	.0312	.0250	.80	865	17.4	17.3	17.3	----	17.6	38
32	.0312	.0275	.88	820	16.0	15.7	15.8	16.1	16.3	40
33	.0310	.0277	.88	825	16.0	15.7	15.8	16.1	16.4	40
34	.0322	.0318	.99	855	16.6	16.3	16.6	16.5	16.8	40
35	.0322	.0318	.99	860	16.7	16.5	16.7	16.7	17.1	40
36	.0311	.0250	.80	865	17.4	17.3	17.3	----	17.4	40
37	.0322	.0301	.94	870	14.2	14.0	14.1	14.2	14.3	40
38	.0307	.025	.82	865	17.4	17.3	17.3	----	17.4	41
39	.0315	.0276	.88	815	15.9	15.6	15.7	17.1	17.3	42
40	.0320	.0320	1.00	870	14.3	14.1	14.2	14.3	14.4	42
41	.0315	.0305	.97	860	16.6	16.4	16.6	16.5	17.0	42
42	.0305	.0277	.91	865	17.4	17.3	17.2	----	17.3	43
43	.0315	.0283	.89	825	16.4	15.6	15.7	16.3	16.1	43
44	.0408	.0352	.86	815	15.9	15.7	15.9	16.7	16.3	24
45	.0415	.0400	.96	870	14.5	14.4	14.6	15.1	14.9	24
46	.0400	.0387	.96	850	16.9	16.8	17.2	17.3	17.2	24
47	.0390	.0374	.96	825	14.2	14.1	14.5	14.6	14.6	24
48	.0405	.0375	.92	850	16.9	16.8	17.1	17.2	17.1	26
49	.0390	.0375	.96	830	14.1	14.1	14.4	14.5	14.5	26
50	.0405	.0391	.96	860	17.1	17.0	17.2	17.5	17.4	28
51	.0390	.0380	.98	835	14.1	14.0	14.3	14.5	14.4	28
52	.0405	.0397	.98	860	17.2	17.1	17.4	17.6	17.4	30
53	.0390	.0375	.96	835	14.1	14.0	14.4	14.6	14.6	30
54	.0415	.0352	.85	865	17.2	17.1	17.4	17.4	17.5	35

Point identi-fication	Liquid mass flow rate, w_T, lb/sec	Vapor mass flow rate, w_g, lb/sec	Inlet quality, x_o	Inlet temper-ature, T_g, °F	1	8	20	32	45	Condensing length, $l_c \times 12$, in.
					Static pressure, $P_S/144$, psia					
55	0.0390	0.0363	0.93	830	14.4	14.2	14.5	14.5	14.7	35
56	.0400	.0364	.91	820	15.9	15.4	15.7	16.2	16.0	36
57	.0400	.0340	.85	870	17.5	17.4	17.6	17.6	17.7	37
58	.0396	.0380	.96	830	14.5	14.3	14.6	14.7	14.8	37
59	.0400	.0367	.92	815	15.8	15.9	15.6	16.0	16.0	39
60	.0408	.0362	.89	870	17.6	17.9	17.5	17.6	17.7	39
61	.0390	.0364	.93	825	14.6	14.2	14.6	14.7	14.9	39
62	.0397	.0356	.90	820	16.5	16.1	16.2	16.7	17.0	40
63	.039	.0382	.98	830	14.4	14.3	14.5	14.6	14.7	40
64	.0408	.0350	.86	860	17.9	17.8	17.9	18.0	18.1	41
65	.0390	.0375	.96	825	14.4	14.3	14.5	14.6	14.8	42
66	.0390	.0375	.96	845	14.2	14.1	14.2	14.5	14.6	43
67	.0415	.0375	.90	870	18.0	17.8	18.0	18.0	18.0	43
68	.0412	.0368	.90	810	16.0	15.4	15.8	16.2	16.0	43
69	.0390	.0376	.96	825	14.9	14.7	14.6	15.0	15.2	44
70	.0512	.0469	.92	805	16.2	16.0	16.2	17.0	16.8	22
71	.0510	.0498	.98	830	17.3	17.4	17.8	17.8	----	24
72	.0507	.0478	.94	805	16.4	16.0	16.4	17.1	16.9	24
73	.0522	.0513	.98	850	18.0	17.8	18.3	18.3	18.6	24
74	.0528	.0510	.96	825	17.7	17.7	18.2	----	18.4	24
75	.0507	.0461	.91	800	16.4	16.2	16.5	17.2	17.0	26
76	.0520	.0510	.98	835	17.4	17.4	17.9	17.9	----	↓
77	.0520	.0520	1.00	850	18.0	17.7	18.1	18.2	18.4	↓
78	.0490	.0480	.98	815	14.1	14.1	14.6	14.6	14.8	↓
79	.0525	.0500	.95	835	17.5	17.4	17.9	----	18.1	↓
80	.0485	.0462	.95	815	14.4	14.4	14.9	15.0	15.2	27
81	.0520	.0501	.96	850	18.0	17.7	17.8	18.2	18.4	28
82	.0515	.0490	.95	840	17.4	17.4	17.6	17.8	----	28
83	.0502	.0460	.92	800	16.7	16.3	16.8	17.5	17.1	28
84	.0540	.0520	.96	845	17.5	17.4	17.8	----	18.2	28
85	.0540	.0513	.95	850	17.5	17.4	17.8	----	18.2	29
86	.0530	.0520	.98	850	17.4	17.3	17.6	----	18.1	29
87	.0520	.0510	.98	850	17.7	17.6	17.9	18.3	----	30
88	.0505	.0500	.99	845	17.5	17.5	17.8	18.0	----	30
89	.0507	.0469	.92	800	16.6	16.8	17.1	17.6	17.4	30
90	.0485	.0472	.97	815	14.0	14.0	14.4	14.5	14.6	30
91	.0515	.0505	.98	855	17.8	17.5	17.8	18.0	18.2	30
92	.0502	.0458	.92	800	19.4	19.0	19.3	19.9	19.5	35
93	.0535	.0518	.97	845	18.2	17.8	18.0	18.3	18.6	35
94	.0515	.0495	.96	885	17.5	17.2	17.4	17.7	17.9	35
95	.0530	.0515	.97	860	17.6	17.4	17.6	----	18.3	35
96	.0485	.0472	.97	850	16.4	16.2	16.4	16.8	16.8	36
97	.0510	.0498	.98	885	17.5	17.2	17.3	17.6	17.9	37
98	.0534	.0505	.95	865	17.6	17.4	17.6	----	18.3	37
99	.0520	.0476	.92	870	18.6	17.9	18.6	18.8	18.8	38
100	.0510	.0500	.98	880	14.6	14.5	14.8	15.3	15.4	39
101	.0515	.0497	.96	880	17.8	17.5	17.6	17.9	18.2	↓
102	.0520	.0481	.92	870	16.5	16.4	16.4	16.6	16.8	↓
103	.0540	.0520	.96	875	17.6	17.5	17.6	----	18.3	↓
104	.0520	.0510	.98	825	17.0	16.7	16.8	17.0	17.4	↓
105	.0515	.0498	.97	875	17.6	17.2	17.4	17.6	17.8	41
106	.0520	.0500	.96	830	17.0	16.7	16.8	17.0	17.4	41
107	.0530	.0500	.94	880	17.5	17.5	17.5	----	18.2	41
108	.0515	.0502	.97	865	18.0	17.7	17.8	18.3	18.3	43
109	.0540	.0510	.94	880	18.5	18.3	18.2	----	18.8	43

"The aeronautical and space activities of the United States shall be conducted so as to contribute . . . to the expansion of human knowledge of phenomena in the atmosphere and space. The Administration shall provide for the widest practicable and appropriate dissemination of information concerning its activities and the results thereof."

—NATIONAL AERONAUTICS AND SPACE ACT OF 1958

NASA SCIENTIFIC AND TECHNICAL PUBLICATIONS

TECHNICAL REPORTS: Scientific and technical information considered important, complete, and a lasting contribution to existing knowledge.

TECHNICAL NOTES: Information less broad in scope but nevertheless of importance as a contribution to existing knowledge.

TECHNICAL MEMORANDUMS: Information receiving limited distribution because of preliminary data, security classification, or other reasons.

CONTRACTOR REPORTS: Technical information generated in connection with a NASA contract or grant and released under NASA auspices.

TECHNICAL TRANSLATIONS: Information published in a foreign language considered to merit NASA distribution in English.

TECHNICAL REPRINTS: Information derived from NASA activities and initially published in the form of journal articles.

SPECIAL PUBLICATIONS: Information derived from or of value to NASA activities but not necessarily reporting the results of individual NASA-programmed scientific efforts. Publications include conference proceedings, monographs, data compilations, handbooks, sourcebooks, and special bibliographies.

Details on the availability of these publications may be obtained from:

SCIENTIFIC AND TECHNICAL INFORMATION DIVISION

NATIONAL AERONAUTICS AND SPACE ADMINISTRATION

Washington, D.C. 20546